Thermodynamic and structural properties of mixed colloids represented by a hard-core two-Yukawa mixture model fluid: Monte Carlo simulations and an analytical theory

Yang-Xin Yu[a] and Lin Jin
Department of Chemical Engineering, Tsinghua University, Beijing 100084, People's Republic of China and State Key Laboratory of Chemical Engineering, Tsinghua University, Beijing 100084, People's Republic of China

(Received 8 October 2007; accepted 29 October 2007; published online 3 January 2008)

The interaction between colloidal particles is well represented by a hard-core two-Yukawa potential. In order to assess the accuracy of theoretical predictions for the thermodynamic and structural properties of mixed colloids, standard Monte Carlo simulations are carried out for the hard-core two-Yukawa mixtures. In the simulations, one range parameter in the two-Yukawa potential is taken as 1.8 or 2.8647, and another is taken as 4, 8, or 13.5485. Both attractive and repulsive dominant cases of the potential outside the hard core are considered. The effects of temperature, density, composition, size and energy parameter ratios on internal energy, compressibility factor, and radial distribution function are investigated extensively. Theoretical calculations are performed in the framework of analytical solution for the Ornstein-Zernike equation with the first-order mean spherical approximation (FMSA). Our analysis shows that the FMSA is very accurate for the prediction of the compressibility factor of the hard-core two-Yukawa mixtures at all conditions studied. The FMSA generally predicts accurate internal energy, but overestimates the internal energy of the systems at lower temperatures. Furthermore, we found that a simplified exponential version of the FMSA predicts fairly good radial distribution function at contact for the mixed two-Yukawa fluids. The comparison of the theoretical compressibility factor with that from the Monte Carlo simulations suggests that the FMSA can be used to investigate the fluid-fluid equilibria of hard-core two-Yukawa mixtures. © *2008 American Institute of Physics*. [DOI: 10.1063/1.2815802]

I. INTRODUCTION

The various interactions between atoms and molecules govern the structural and thermodynamic properties of fluids. In principle, they can be calculated using quantum mechanics, but such calculations are far from trivial, requiring electron correlation and large basis sets.[1] In practice, we model the interatomic potential curve using a simple empirical expression such as square-well, Lennard-Jones, Yukawa potentials, etc. Among the empirical potentials, the fluid with multi-Yukawa potential is able to simulate real systems without losing generality. It can be successfully applied to a wide variety of real systems including charge-stabilized colloids,[2] dusty plasmas,[3] microemulsions,[4] globular proteins,[5,6] and C_{60} fullerene systems.[7] A charged colloidal particle system with a short-range attraction and a long-range electrostatic repulsion has been successfully described on the basis of the well-known Derjaguin-Laudan-Verwey-Overbeek (DLVO) theory, which is also expressed as a Yukawa potential.[5] The hard-core two-Yukawa (HCTY) potential has been used to predict thermodynamic and diffusion properties of globular proteins in aqueous electrolyte solution[5,8] and to explain the small-angle neutron scattering spectra of cytochrome C protein solutions at moderate concentrations.[9] In addition, the Lennard-Jones potential can also be well approximated by a hard-core repulsion with two-Yukawa tails.[10]

An obvious advantage of Yukawa potential is that the analytical expressions for structural and thermodynamic properties of fluid are easy to obtain. Waisman[11] obtained the analytical solution of the Ornstein-Zernike (OZ) integral with the mean spherical approximation (MSA) for one-Yukawa potential in 1973. Then the analytical solution based on the MSA is extended to a system of particles interacting with a multi-Yukawa potential by Blum and Høye.[12] Most of the previous studies on pure Yukawa fluid concern some sort of numerical techniques leading to the convergence problems.[2] Using the inverse temperature expansion of the MSA free energy up to the fifth term, Henderson *et al.*[13] obtained an analytical equation of state. Another simple form of pressure equation for the one-Yukawa fluid is proposed in terms of a scaling parameter Γ.[14] By performing an infinite expansion of the free energy in terms of the inverse temperature,[15] the theory of Henderson *et al.*[13] can be made more accurate for equation of state. Recently, Lin *et al.*[16] revised the excess entropy for the two-Yukawa fluid and obtained an equation of state that can be used to accurately predict the thermodynamic properties for the HCTY fluid. In recent years, a numerous computer simulation data have been used to test the prediction accuracy of the integral equation theory and perturbation theory for the phase transition,

[a]Author to whom correspondence should be addressed. Electronic mail: yangxyu@mail.tsinghua.edu.cn

 © 2008 American Institute of Physics

Author complimentary copy. Redistribution subject to AIP license or copyright, see http://jcp.aip.org/jcp/copyright.jsp

TABLE I. Radial distribution function at contact, internal energy, and compressibility factor of hard-core two-Yukawa fluid mixture from Monte Carlo simulations for $\sigma_2/\sigma_1=0.5$, $\varepsilon_2/\varepsilon_1=0.5$, $\lambda_{1,1}=\lambda_{1,2}=\lambda_{1,12}=1.8$, $\lambda_{2,1}=4.0$, and $k_1=k_2=1.0$ (case 1).

T^*	x_1	ρ^*	$g_{11}(\sigma_1)$	$g_{22}(\sigma_2)$	$g_{12}(\sigma_{12})$	U/Nk_BT	Z
1.5	0.5	0.3	4.249	2.113	2.839	−1.058	0.537
		0.5	4.118	2.292	2.979	−1.693	0.333
		0.7	3.675	2.403	2.955	−2.174	0.186
		0.9	3.487	2.528	2.989	−2.661	0.083
		1.1	3.690	2.756	3.203	−3.248	0.136
		1.3	4.234	3.114	3.602	−3.915	0.522
2.0	0.5	0.3	2.690	1.750	2.130	−0.649	0.778
		0.5	2.708	1.879	2.243	−1.064	0.691
		0.7	2.790	2.037	2.385	−1.479	0.669
		0.9	3.001	2.242	2.592	−1.918	0.755
		1.1	3.395	2.513	2.906	−2.397	1.039
		1.3	4.041	2.893	3.359	−2.915	1.678
3.0	0.25	0.5	1.994	1.518	1.733	−0.346	1.023
		0.7	2.076	1.602	1.818	−0.488	1.064
		0.9	2.176	1.701	1.925	−0.635	1.132
		1.1	2.318	1.815	2.052	−0.786	1.234
		1.3	2.512	1.948	2.210	−0.945	1.387
3.0	0.5	0.3	2.025	1.512	1.727	−0.395	0.986
		0.5	2.162	1.643	1.878	−0.665	1.043
		0.7	2.374	1.814	2.065	−0.948	1.184
		0.9	2.706	2.047	2.327	−1.252	1.471
		1.1	3.194	2.337	2.682	−1.581	1.990
		1.3	3.917	2.732	3.176	−1.934	2.903
3.0	0.75	0.3	2.116	1.587	1.806	−0.636	0.973
		0.5	2.383	1.777	2.054	−1.081	1.132
		0.7	2.852	2.117	2.418	−1.568	1.592
		0.9	3.641	2.571	2.978	−2.112	2.651
		1.1	5.000	3.281	3.879	−2.714	4.960
		1.3	7.478	4.521	5.417	−3.369	9.969

and the thermodynamic and structural properties for the attractive and repulsive one-Yukawa fluids[17,18] and the HCTY fluid.[19–21]

It should be mentioned that the analytical solution of the OZ equation with the first-order mean spherical approximation (FMSA) proposed by Tang[10] and Tang *et al.*[20] has a relatively simpler expression for the thermodynamic properties of hard-core multi-Yukawa fluid, and it also predicts the compressibility factor of HCTY fluid very well.[20] This FMSA theory has been recently applied to calculate the concentration dependence of the osmotic pressure for four globular proteins in aqueous electrolyte solutions.[5]

In contrast to the pure fluid with Yukawa potential, few works have been reported for HCTY fluid mixture. Theoretically, the analytical solution of the OZ equation with the MSA derived by Blum and Høye[12] has been extended to the hard-core multi-Yukawa mixtures by Arrieta *et al.*,[22] while no computer simulation is carried out to test this analytical results for multi-Yukawa mixtures. Recently, Scholl-Paschinger *et al.*[23] predicted the phase diagram for the binary symmetric hard-core Yukawa mixture using a self-consistent OZ equation and compared their numerical results with the Monte Carlo (MC) simulation data. Giacometti *et al.*[24] compared the structural properties of binary one-Yukawa mixtures from the hypernetted-chain and Percus-Yevick approximations with the corresponding simulation data. Among the various approximations for the OZ equation, only MSA gives analytical solution for the multi-Yukawa mixtures. However, in the MSA approach, the correct coefficients of the analytical form have to be obtained by solving a group of nonlinear equations, and the complexity is increased with the number of terms in the multi-Yukawa potential and the components in the system. Fortunately, the FMSA can avoid solving the group of nonlinear equations and still give analytical expression of Helmholtz free energy. Therefore, the FMSA is adopted here to retrieve the thermodynamic and structural properties of mixed colloids.

Colloidal dispersion systems include blood, proteins in solution, milk, ink, etc. They are very important for biology, industrial production, and our everyday life.[25] Since these systems are generally polydisperse in size and in interaction energy, we investigate here the thermodynamic and structural properties for binary mixed colloids as a starting point. We model the mixed colloidal system as a binary HCTY mixture, where the first Yukawa tail is used to simulate the van der Waals interaction and the second Yukawa tail is for the

Author complimentary copy. Redistribution subject to AIP license or copyright, see http://jcp.aip.org/jcp/copyright.jsp

TABLE II. Radial distribution function at contact, internal energy, and compressibility factor of hard-core two-Yukawa fluid mixture from Monte Carlo simulations for $\sigma_2/\sigma_1=0.5$, $\varepsilon_2/\varepsilon_1=0.5$, $\lambda_{1,1}=\lambda_{1,2}=\lambda_{1,12}=1.8$, $\lambda_{2,1}=8.0$, and $k_1=k_2=-6.0$ (case 2).

T^*	x_1	ρ^*	$g_{11}(\sigma_1)$	$g_{22}(\sigma_2)$	$g_{12}(\sigma_{12})$	U/Nk_BT	Z
2.0	0.5	0.3	0.123	0.373	0.236	−0.057	1.439
		0.5	0.178	0.469	0.313	−0.037	2.006
		0.7	0.278	0.606	0.432	0.064	2.927
		0.9	0.458	0.803	0.614	0.280	4.344
		1.1	0.777	1.074	0.890	0.645	6.410
		1.3	1.335	1.461	1.307	1.179	9.351
3.0	0.25	0.5	0.288	0.566	0.429	0.034	1.476
		0.7	0.355	0.642	0.504	0.069	1.769
		0.9	0.452	0.735	0.597	0.121	2.145
		1.1	0.577	0.851	0.713	0.193	2.619
		1.3	0.749	0.986	0.860	0.289	3.213
3.0	0.5	0.3	0.272	0.545	0.409	−0.015	1.436
		0.5	0.373	0.667	0.523	0.017	1.948
		0.7	0.537	0.826	0.679	0.102	2.732
		0.9	0.802	1.043	0.906	0.260	3.900
		1.1	1.218	1.331	1.231	0.509	5.585
		1.3	1.891	1.737	1.696	0.863	7.996
3.0	0.75	0.3	0.315	0.601	0.457	−0.05	1.718
		0.5	0.501	0.798	0.648	0.026	2.787
		0.7	0.855	1.088	0.955	0.260	4.696
		0.9	1.525	1.553	1.466	0.717	7.923
		1.1	2.792	2.247	2.316	1.447	13.250
		1.3	4.282	5.306	3.518	2.433	20.575
6.0	0.5	0.3	0.591	0.794	0.705	0.009	1.419
		0.5	0.760	0.936	0.854	0.036	1.862
		0.7	1.007	1.113	1.053	0.089	2.505
		0.9	1.362	1.349	1.324	0.175	3.430
		1.1	1.877	1.649	1.690	0.303	4.751
		1.3	2.635	2.065	2.192	0.477	6.646

DLVO interaction between charge-stabilized colloids. We reformulate the Helmholtz free energy, internal energy, and radial distribution function at contact for the HCTY mixture within the framework of the FMSA. To test the performance of the FMSA, standard canonical ensemble MC simulations have been carried out to obtain the radial distribution function, compressibility factor, and internal energy for the binary HCTY mixture at different temperatures, densities, compositions, and energy parameter ratios.

In what follows, we present the MC simulation method to calculate structural and thermodynamic properties of binary HCTY mixtures in Sec. II. We describe the analytical theory in Sec. III. We present and discuss numerical results for the compressibility factor, internal energy, and radial distribution function in Sec. IV, and some conclusions are given in Sec. V.

II. MONTE CARLO SIMULATIONS

Canonical ensemble (*NVT*) Monte Carlo simulations were performed for the structural and thermodynamic properties of binary HCTY fluid mixtures under various conditions, where N is the number of particles, T is the absolute temperature, and V is the volume of the system. The interactions between the HCTY particles are described as

$$u_{ij}(r)=\begin{cases}\infty, & r\leqslant\sigma_{ij}\\ -\sum_{k=1}^{2}\varepsilon_{k,ij}\dfrac{\exp[-\lambda_{k,ij}(r/\sigma_{ij}-1)]}{r/\sigma_{ij}}, & r>\sigma_{ij},\end{cases}\tag{1}$$

where r is the center-to-center distance between two interacting particles, σ_{ii} is the hard-core diameter of particle i, $\varepsilon_{k,ij}$ and $\lambda_{k,ij}$ represent, respectively, the potential energy parameter and the screen length of kth Yukawa tail. The first Yukawa tail represents the van der Waals interaction, and in this case, we assume $\lambda_{1,ii}=\lambda_{1,jj}=\lambda_{1,ij}$. Since the second Yukawa tail represents the DLVO theory, we can obtain $\lambda_{2,ii}/\sigma_{ii}=\lambda_{2,jj}/\sigma_{jj}=\lambda_{2,ij}/\sigma_{ij}$ from the fact that the two kinds of colloids are in the same electrolyte solution. If we let $\varepsilon_{1,ij}=\varepsilon_{ij}$ and $\varepsilon_{2,ij}=k_{ij}\varepsilon_{ij}$, the Lorentz-Berthelot combining rule can be used to obtain the cross parameters of energy and hard-core diameter, i.e., $\varepsilon_{ij}=(\varepsilon_i\varepsilon_j)^{1/2}$, $k_{ij}=(k_ik_j)^{1/2}(|k_i|/k_i)$, and $\sigma_{ij}=(\sigma_i+\sigma_j)/2$. In all cases studied, we regarded $\sigma_{ii}=\sigma_i$, $\varepsilon_{ii}=\varepsilon_i$, $k_{ii}=k_i$, $\lambda_{1,ii}=\lambda_{1,i}$, and $\lambda_{2,ii}=\lambda_{2,i}$.

In the simulation, the internal energy is obtained through $U=U_s+U_l$, where U_s is the internal energy averaged from

Author complimentary copy. Redistribution subject to AIP license or copyright, see http://jcp.aip.org/jcp/copyright.jsp

TABLE III. Radial distribution function at contact, internal energy, and compressibility factor of hard-core two-Yukawa fluid mixture from Monte Carlo simulations for $\sigma_2/\sigma_1=0.5$, $\varepsilon_2/\varepsilon_1=0.5$, $\lambda_{1,1}=\lambda_{1,2}=\lambda_{1,12}=1.8$, $\lambda_{2,1}=8.0$, and $k_1=k_2=-12.0$ (case 3).

T^*	x_1	ρ^*	$g_{11}(\sigma_1)$	$g_{22}(\sigma_2)$	$g_{12}(\sigma_{12})$	U/Nk_BT	Z
4.0	0.5	0.3	0.104	0.337	0.206	0.094	1.617
		0.5	0.160	0.434	0.281	0.236	2.340
		0.7	0.261	0.570	0.399	0.477	3.447
		0.9	0.441	0.758	0.578	0.849	5.058
		1.1	0.765	1.029	0.849	1.379	7.336
		1.3	1.326	1.407	1.260	2.088	10.486
6.0	0.25	0.5	0.264	0.530	0.395	0.122	1.579
		0.7	0.337	0.609	0.470	0.198	1.925
		0.9	0.433	0.703	0.564	0.295	2.357
		1.1	0.564	0.814	0.679	0.415	2.892
		1.3	0.739	0.952	0.827	0.562	3.552
6.0	0.5	0.3	0.245	0.509	0.375	0.089	1.558
		0.5	0.348	0.631	0.486	0.204	2.173
		0.7	0.516	0.788	0.645	0.383	3.078
		0.9	0.780	1.005	0.871	0.644	4.375
		1.1	1.204	1.298	1.196	1.003	6.201
		1.3	1.876	1.688	1.660	1.474	8.748
6.0	0.75	0.3	0.287	0.567	0.425	0.128	1.930
		0.5	0.475	0.756	0.614	0.353	3.187
		0.7	0.830	1.048	0.918	0.757	5.310
		0.9	1.505	1.506	1.426	1.398	8.767
		1.1	2.785	2.236	2.275	2.323	14.344
		1.3	3.873	6.777	3.229	3.474	21.127
8.0	0.5	0.3	0.371	0.628	0.505	0.080	1.522
		0.5	0.509	0.758	0.637	0.175	2.080
		0.7	0.715	0.928	0.815	0.317	2.882
		0.9	1.029	1.153	1.065	0.518	4.024
		1.1	1.503	1.456	1.408	0.789	5.626
		1.3	2.226	1.857	1.896	1.139	7.883

the MC simulation with the cutoff radius of r_c, and U_l is the long-range correction of the internal energy derived from the energy equation.[26]

$$U_s = \left\langle \sum_{i=1}^{N} \sum_{j=i+1}^{N} u_{ij}(r_{ij}) \right\rangle_{\text{ens}} \quad (\sigma_{ij} < r_{ij} \leqslant r_c), \tag{2}$$

$$U_l = -2\pi\rho N \sum_{i=1}^{2} \sum_{j=1}^{2} x_i x_j D_{ij} \sigma_{ij}^3, \tag{3}$$

where $\langle\ \rangle_{\text{ens}}$ represents the ensemble average, ρ is the total number density of the system, and x_i is the molar fraction of component i. Equation (3) is obtained from energy equation by assuming the radial distribution function $g_{ij}(r)=1$ when $r>r_c$. The coefficient D_{ij} is expressed as

$$D_{ij} = \sum_{k=1}^{2} \varepsilon_{k,ij} \left(\frac{r_c}{\lambda_{k,ij}\sigma_{ij}} + \frac{1}{\lambda_{k,ij}^2} \right) \exp\left[-\lambda_{k,ij} \left(\frac{r_c}{\sigma_{ij}} - 1 \right) \right]. \tag{4}$$

The compressibility factor Z of the binary HCTY mixture is obtained based on the pressure equation,[26]

$$Z = 1 - \frac{1}{6\rho k_B T} \sum_i \sum_j \rho_i \rho_j \int_0^\infty \frac{du_{ij}(r)}{dr} g_{ij}(r) 4\pi r^3 dr, \tag{5}$$

where k_B is the Boltzmann constant. The integral in the right-hand side can be obtained from the sum of the integrations in the three intervals, i.e., $r=\sigma_{ij}$, $\sigma_{ij}<r\leqslant r_c$, and $r>r_c$. Thus Eq. (5) can be written as

$$Z = 1 + Z_h + Z_s + Z_l, \tag{6}$$

where

$$Z_h = \frac{2\pi\rho}{3} \sum_{i=1}^{2} \sum_{j=1}^{2} x_i x_j g_{ij}(\sigma_{ij}) \sigma_{ij}^3, \tag{7}$$

$$Z_s = \left\langle -\frac{1}{3Nk_BT} \sum_{i=1}^{N} \sum_{j=i+1}^{N} r_{ij} \frac{\partial u_{ij}(r)}{\partial r}\bigg|_{r_{ij}} \right\rangle_{\text{ens}} \quad (\sigma_{ij} < r_{ij} \leqslant r_c), \tag{8}$$

$$Z_l = -\frac{2\pi\rho}{3k_BT} \sum_{i=1}^{2} \sum_{j=1}^{2} x_i x_j C_{ij} \sigma_{ij}^3, \tag{9}$$

with

Author complimentary copy. Redistribution subject to AIP license or copyright, see http://jcp.aip.org/jcp/copyright.jsp

TABLE IV. Effect of particle size on radial distribution function at contact, internal energy, and compressibility factor of hard-core two-Yukawa fluid mixture from Monte Carlo simulations for $x_1=0.5$, $\varepsilon_2/\varepsilon_1=0.5$, $\lambda_{1,1}=\lambda_{1,2}=\lambda_{1,12}=1.8$, $\lambda_{2,1}=4.0$, and $k_1=k_2=1.0$ (case 1).

T^*	σ_2/σ_1	ρ^*	$g_{11}(\sigma_1)$	$g_{22}(\sigma_2)$	$g_{12}(\sigma_{12})$	U/Nk_BT	Z
3.0	0.25	0.5	2.113	1.530	1.778	−0.549	0.970
		0.7	2.270	1.661	1.894	−0.778	1.026
		0.9	2.506	1.799	2.042	−1.021	1.155
		1.1	2.840	1.979	2.217	−1.281	1.395
		1.3	3.322	2.194	2.450	−1.558	1.819
3.0	0.75	0.3	2.114	1.595	1.803	−0.501	1.062
		0.5	2.355	1.830	2.044	−0.853	1.255
		0.7	2.750	2.177	2.418	−1.235	1.688
		0.9	3.391	2.690	2.989	−1.656	2.570
		1.1	4.423	3.470	3.877	−2.117	4.274
		1.3	6.152	4.690	5.326	−2.617	7.586

TABLE V. Effect of particle size on radial distribution function at contact, internal energy, and compressibility factor of hard-core two-Yukawa fluid mixture from Monte Carlo simulations for $x_1=0.5$, $\varepsilon_2/\varepsilon_1=0.5$, $\lambda_{1,1}=\lambda_{1,2}=\lambda_{1,12}=1.8$, $\lambda_{2,1}=8.0$, and $k_1=k_2=-6.0$ (case 2).

T^*	σ_2/σ_1	ρ^*	$g_{11}(\sigma_1)$	$g_{22}(\sigma_2)$	$g_{12}(\sigma_{12})$	U/Nk_BT	Z
3.0	0.25	0.5	0.336	0.551	0.437	0.001	1.672
		0.7	0.460	0.634	0.524	0.051	2.196
		0.9	0.649	0.738	0.638	0.148	2.954
		1.1	0.932	0.866	0.785	0.305	4.020
		1.3	1.364	1.028	0.984	0.534	5.497
3.0	0.75	0.3	0.300	0.629	0.466	−0.022	1.659
		0.5	0.454	0.853	0.667	0.041	2.543
		0.7	0.731	1.204	0.997	0.212	4.033
		0.9	1.226	1.740	1.536	0.528	6.432
		1.1	2.106	2.566	2.413	1.021	10.208
		1.3	3.736	3.923	3.922	1.723	16.300

TABLE VI. Effect of energy parameter on radial distribution function at contact, internal energy, and compressibility factor of hard-core two-Yukawa fluid mixture from Monte Carlo simulations for $x_1=0.5$, $\sigma_2/\sigma_1=0.5$, $\lambda_{1,1}=\lambda_{1,2}=\lambda_{1,12}=1.8$, $\lambda_{2,1}=4.0$, and $k_1=k_2=1.0$ (case 1).

T^*	$\varepsilon_2/\varepsilon_1$	ρ^*	$g_{11}(\sigma_1)$	$g_{22}(\sigma_2)$	$g_{12}(\sigma_{12})$	U/Nk_BT	Z
3.0	0.25	0.3	2.055	1.285	1.540	−0.339	1.041
		0.5	2.198	1.434	1.692	−0.571	1.138
		0.7	2.425	1.607	1.896	−0.817	1.328
		0.9	2.766	1.838	2.166	−1.079	1.668
		1.1	3.263	2.127	2.538	−1.363	2.250
		1.3	3.991	2.503	3.045	−1.670	3.227
3.0	0.75	0.3	2.019	1.764	1.891	−0.444	0.942
		0.5	2.143	1.902	2.024	−0.745	0.966
		0.7	2.345	2.090	2.201	−1.061	1.070
		0.9	2.662	2.312	2.442	−1.398	1.308
		1.1	3.144	2.615	2.783	−1.762	1.779
		1.3	3.859	3.015	3.265	−2.153	2.636

Author complimentary copy. Redistribution subject to AIP license or copyright, see http://jcp.aip.org/jcp/copyright.jsp

TABLE VII. Effect of energy parameter on radial distribution function at contact, internal energy, and compressibility factor of hard-core two-Yukawa fluid mixture from Monte Carlo simulations for $x_1=0.5$, $\sigma_2/\sigma_1=0.5$, $\lambda_{1,1}=\lambda_{1,2}=\lambda_{1,12}=1.8$, $\lambda_{2,1}=8.0$, and $k_1=k_2=-6.0$ (case 2).

T^*	$\varepsilon_2/\varepsilon_1$	ρ^*	$g_{11}(\sigma_1)$	$g_{22}(\sigma_2)$	$g_{12}(\sigma_{12})$	U/Nk_BT	Z
3.0	0.25	0.3	0.268	0.804	0.567	−0.017	1.422
		0.5	0.367	0.954	0.705	0.007	1.908
		0.7	0.522	1.152	0.898	0.076	2.648
		0.9	0.769	1.408	1.170	0.207	3.744
		1.1	1.165	1.740	1.542	0.416	5.333
		1.3	1.797	2.186	2.062	0.717	7.606
3.0	0.75	0.3	0.273	0.370	0.318	−0.015	1.446
		0.5	0.380	0.454	0.411	0.020	1.977
		0.7	0.549	0.578	0.548	0.116	2.797
		0.9	0.822	0.753	0.748	0.294	4.018
		1.1	1.262	0.993	1.040	0.573	5.790
		1.3	1.960	1.341	1.472	0.970	8.303

$$C_{ij}=\sum_{k=1}^{2}\varepsilon_{k,ij}\left(\frac{r_c^2}{\sigma_{ij}^2}+\frac{3r_c}{\lambda_{k,ij}\sigma_{ij}}+\frac{3}{\lambda_{k,ij}^2}\right)\exp\left[-\lambda_{k,ij}\left(\frac{r_c}{\sigma_{ij}}-1\right)\right]. \tag{10}$$

From Eqs. (6)–(10), one can see that Z_l can be calculated directly, and Z_s can be averaged from the MC simulation. To obtain Z_h, we need the values of radial distribution function at contact. In this work, they are extrapolated from the radial distribution functions in the vicinity of contact.

In the *NVT* MC simulations, $N=500$ particles were placed in a cubic box of length L and the standard Metropolis algorithm with periodic boundary conditions were applied. In each simulation, about 5×10^4 MC cycles (2.5×10^7 configurations) were used to equilibrate the system. After equilibration, internal energy, compressibility factor, and radial distribution function were obtained using appropriate averages over the subsequent 9.5×10^5 MC cycles. In each simulation, the value of cutoff radius was selected to $3.6\sigma_1\leqslant r_c\leqslant5.9\sigma_1$, depending on the density of the system.

The MC simulations were carried out for the binary HCTY mixture under various conditions. The studied parameters in the HCTY potential are designed as the following cases:

$$\lambda_{1,1}=1.8,\quad \lambda_{2,1}=4.0,\quad \text{and } k_1=k_2=1.0\quad \text{(Case 1)},$$

$$\lambda_{1,1}=1.8,\quad \lambda_{2,1}=8.0,\quad \text{and } k_1=k_2=-6.0\quad \text{(Case 2)},$$

$$\lambda_{1,1}=1.8,\quad \lambda_{2,1}=8.0,\quad \text{and } k_1=k_2=-12.0\ \text{(Case 3)},$$

$$\lambda_{1,1}=2.8647,\quad \lambda_{2,1}=13.5485,\quad \text{and } k_1=k_2=-1.4466\ \text{(Case 4)}.$$

In cases 1–3, we select $\lambda_{1,1}=1.8$ due to the fact that it is frequently used to represent the dispersive interaction (with Yukawa potential) between colloidal particles.[8] In case 1, there is no repulsive interaction outside the hard core. Cases 2 and 3 are examples for the interaction between real charged protein molecules in a binary mixture, and case 4 represents the Yukawa potential that mimics the behavior of the well-known Lennard-Jones potential.

III. ANALYTICAL THEORY

The integral equation theory with the FMSA has been proposed to model attractive hard-core one-Yukawa and

TABLE VIII. Radial distribution function at contact, internal energy, and compressibility factor of hard-core two-Yukawa fluid mixture from Monte Carlo simulations for $\varepsilon_2/\varepsilon_1=0.5$, $\sigma_2/\sigma_1=0.5$, $\lambda_{1,1}=\lambda_{1,2}=\lambda_{1,12}=2.8647$, $\lambda_{2,1}=13.5485$, and $k_1=k_2=-1.4466$ (case 4).

T^*	x_1	ρ^*	$g_{11}(\sigma_1)$	$g_{22}(\sigma_2)$	$g_{12}(\sigma_{12})$	U/Nk_BT	Z
0.563	0.5	0.3	0.453	0.755	0.630	−0.619	0.830
		0.5	0.465	0.843	0.692	−0.997	0.815
		0.7	0.501	0.954	0.777	−1.372	0.910
		0.9	0.588	1.113	0.913	−1.762	1.228
		1.1	0.766	1.346	1.132	−2.155	1.981
		1.3	1.096	1.682	1.471	−2.514	3.480
1.5	0.5	0.3	0.841	0.980	0.934	−0.200	1.180
		0.5	0.958	1.101	1.058	−0.339	1.398
		0.7	1.137	1.258	1.230	−0.482	1.754
		0.9	1.394	1.474	1.462	−0.625	2.322
		1.1	1.790	1.752	1.787	−0.764	3.238
		1.3	2.386	2.125	2.237	−0.885	4.690

Author complimentary copy. Redistribution subject to AIP license or copyright, see http://jcp.aip.org/jcp/copyright.jsp

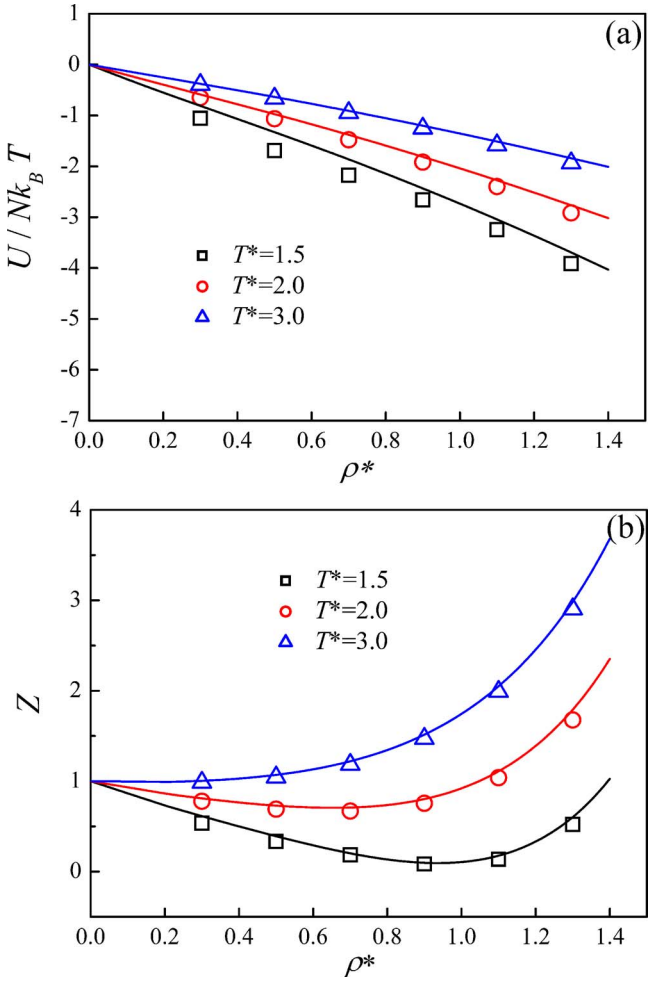

FIG. 1. (Color online) Comparison of (a) internal energy and (b) compressibility factor of binary HCTY mixtures as a function of density from the FMSA and Monte Carlo simulations for $\sigma_2/\sigma_1=0.5$, $\varepsilon_2/\varepsilon_1=0.5$, $x_1=0.5$, $\lambda_{1,1}=\lambda_{1,2}=\lambda_{1,12}=1.8$, $\lambda_{2,1}=4.0$, and $k_1=k_2=1.0$ (case 1). The symbols and solid lines represent the results from MC simulations and theory, respectively.

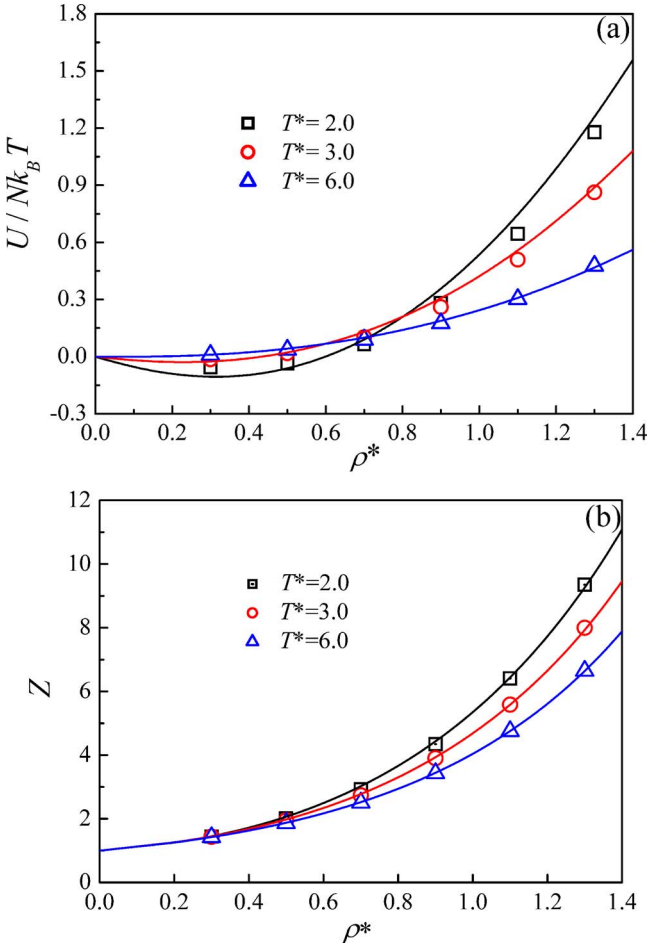

FIG. 2. (Color online) Comparison of (a) internal energy and (b) compressibility factor of binary HCTY mixtures as a function of density from the FMSA and Monte Carlo simulation with $\sigma_2/\sigma_1=0.5$, $\varepsilon_2/\varepsilon_1=0.5$, $x_1=0.5$, $\lambda_{1,1}=\lambda_{1,2}=\lambda_{1,12}=1.8$, $\lambda_{2,1}=8.0$, and $k_1=k_2=-6.0$ (case 2). The meaning of the symbols is the same as in Fig. 1.

multi-Yukawa spheres.[20] Here we systematically apply this approach to mixture fluid and see how well it describes the behavior of the binary HCTY mixtures.

A. Thermodynamic properties

According to the FMSA of Tang,[10] analytical expression for the Helmholtz free energy can be expressed as

$$A^E/Nk_BT = a_0 + a_1 + a_2, \tag{11}$$

where A^E is the total excess Helmholtz free energy of the system, a_0 is the hard-core repulsion contribution, and a_1 and a_2 are the perturbative terms. a_0 is obtained from the Boublik-Mansoori-Carnahan-Starling-Leland (BMCSL) equation of state,[27]

$$a_0 = \frac{1}{\xi_0}\left[\frac{(3\xi_1\xi_2-\xi_2^3/\xi_3^2)}{\Delta}+\frac{\xi_2^3}{\xi_3^2\Delta^2}+\left(\frac{\xi_2^3}{\xi_3^2}\ln\Delta\right)\right]-\ln\Delta, \tag{12}$$

where $\xi_n=\Sigma_i\pi\rho_i\sigma_i^n/6$, $n=0$, 1, 2, and 3, $\Delta=1-\xi_3$. a_1 and a_2 are expressed, respectively, by

$$a_1 = -2\pi\rho\beta\sum_k\sum_i\sum_j x_i x_j \varepsilon_{k,ij}\sigma_{ij}G_{0,ij}(\lambda_{k,ij})e^{\lambda_{k,ij}}, \tag{13}$$

$$a_2 = -\pi\rho\beta\sum_k\sum_i\sum_j x_i x_j \varepsilon_{k,ij}\sigma_{ij}G_{1,ij}(\lambda_{k,ij})e^{\lambda_{k,ij}}, \tag{14}$$

where $\beta=1/k_BT$, $G_{0,ij}(s)$ and $G_{1,ij}(s)$ are, respectively, the reference and the first-order perturbative radial distribution functions in terms of Laplace transform,

$$G_{0,ij}(s) = \frac{e^{-s}}{\Delta\,\det(s)}\left[\frac{\sigma_{ij}^2}{s^2}\left(1+\frac{3\xi_3}{\Delta}\right)+\frac{\sigma_{ij}}{s}\left(\sigma_{ij}+\frac{3\xi_2\sigma_i\sigma_j}{2\Delta}\right)+\frac{\pi\sigma_{ij}}{2\Delta s}\sum_m \rho_m\varphi_1(\sigma_m)(\sigma_m-\sigma_i)(\sigma_m-\sigma_j)\right], \tag{15}$$

$$G_{1,ij}(s) = \sum_\gamma\sum_l\sum_k\sum_m\sum_n \frac{K_{\gamma,lk}B_{ml}(\lambda_{\gamma,lk})B_{nk}(\lambda_{\gamma,lk})}{s+\lambda_{\gamma,lk}} \times B_{mi}(s)B_{nj}(s)\frac{e^{-s}}{2\pi\rho\sqrt{x_i x_j}}, \tag{16}$$

where $\gamma=1,2$, $K_{\gamma,ij}=2\pi\beta\varepsilon_{\gamma,ij}\sigma_{ij}\sqrt{\rho_i\rho_j}$, and $B_{ij}(s)$ is expressed by

Author complimentary copy. Redistribution subject to AIP license or copyright, see http://jcp.aip.org/jcp/copyright.jsp

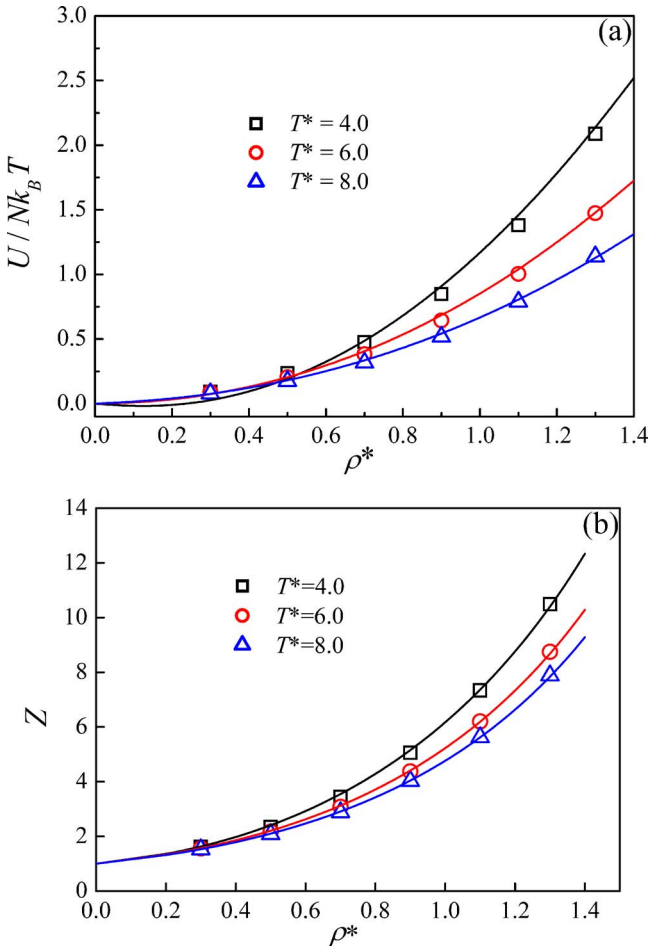

FIG. 3. (Color online) Comparison of (a) internal energy and (b) compressibility factor of binary HCTY mixtures as a function of density from the FMSA and Monte Carlo simulations with $\sigma_2/\sigma_1=0.5$, $\varepsilon_2/\varepsilon_1=0.5$, $x_1=0.5$, $\lambda_{1,1}=\lambda_{1,2}=\lambda_{1,12}=1.8$, $\lambda_{2,1}=8.0$, and $k_1=k_2=-12.0$ (case 3). The meaning of the symbols is the same as in Fig. 1.

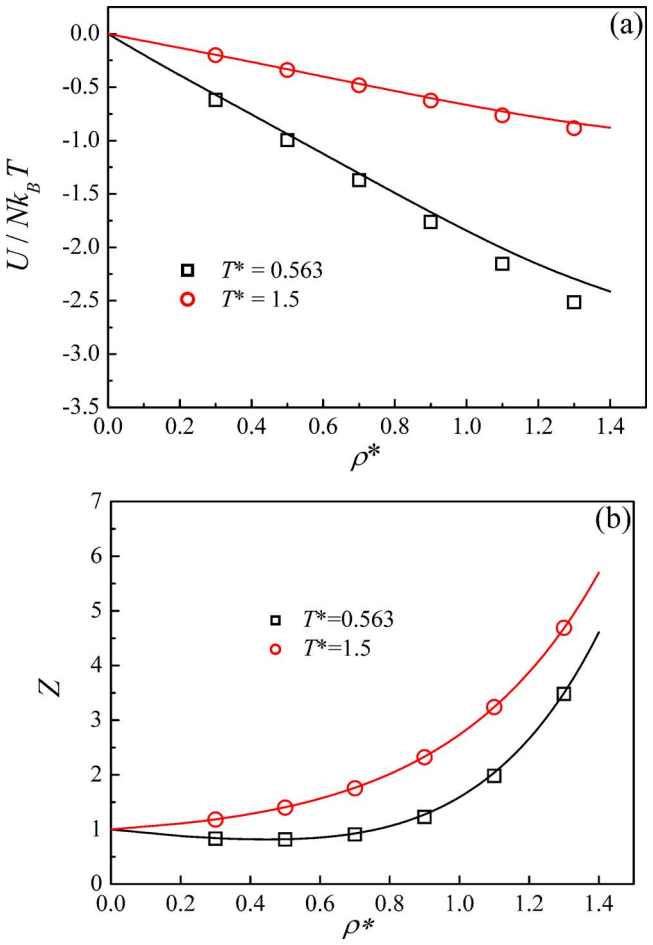

FIG. 4. (Color online) Comparison of (a) internal energy and (b) compressibility factor of binary HCTY mixtures as a function of density from the FMSA and Monte Carlo simulations for $\sigma_2/\sigma_1=0.5$, $\varepsilon_2/\varepsilon_1=0.5$, $x_1=0.5$, $\lambda_{1,1}=\lambda_{1,2}=\lambda_{1,12}=2.8647$, $\lambda_{2,1}=13.5485$, and $k_1=k_2=-1.4466$ (case 4). The meaning of the symbols is the same as in Fig. 1.

$$B_{ij}(s)=\delta_{ij}+2\pi\sqrt{\rho_i\rho_j}\frac{W_{ij}(s)}{\Delta\,\det(s)}, \tag{17}$$

$$W_{ij}(s)=\varphi_2(\sigma_i)\left(1+\frac{3\xi_3}{\Delta}\right)+\varphi_1(\sigma_i)\left(\sigma_{ij}+\frac{3\xi_2\sigma_i\sigma_j}{2\Delta}\right)+\frac{\pi}{2\Delta}\varphi_1(\sigma_i)\sum_m\rho_m\varphi_1(\sigma_m)(\sigma_m-\sigma_i)(\sigma_m-\sigma_j)+\frac{\pi}{2\Delta}\sigma_i^2\sum_m\rho_m\varphi_2(\sigma_m)(\sigma_j-\sigma_m), \tag{18}$$

with

$$\varphi_1(\sigma_i)=\frac{(1-s-e^{-s})\sigma_i^2}{s^2}, \tag{19}$$

$$\varphi_2(\sigma_i)=\frac{(1-s+s^2/2-e^{-s})\sigma_i^3}{s^3}, \tag{20}$$

$$\det(s)=1-\frac{2\pi}{\Delta}\rho\sum_m x_m\varphi_2(\sigma_m)\left(1+\frac{3\xi_3}{\Delta}\right)-\frac{2\pi}{\Delta}\rho\sum_m x_m\varphi_1(\sigma_m)\left(\sigma_m+\frac{3\xi_2\sigma_m^2}{2\Delta}\right)-\frac{\pi^2}{2\Delta^2}\rho^2\sum_m\sum_n x_m x_n\varphi_1(\sigma_m)\varphi_1(\sigma_n)(\sigma_m-\sigma_n)^2. \tag{21}$$

In Eq. (18), δ_{ij} is Kronecker delta function.

The corresponding analytical expressions for the compressibility factor and internal energy can be obtained from the standard thermodynamic relationship,

$$Z=\rho[\partial(A/Nk_BT)/\partial\rho]_{T,N}, \tag{22}$$

and

$$U/Nk_BT=-T[\partial(A/Nk_BT)/\partial T]_{V,N}. \tag{23}$$

Thus we can obtain

Author complimentary copy. Redistribution subject to AIP license or copyright, see http://jcp.aip.org/jcp/copyright.jsp

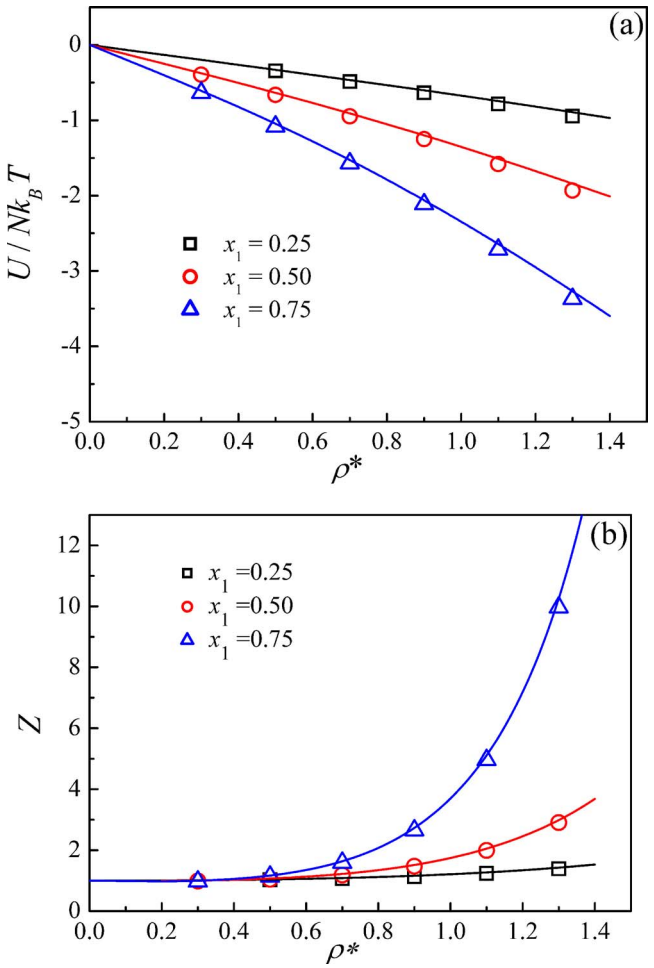

FIG. 5. (Color online) Comparison of (a) internal energy and (b) compressibility factor of binary HCTY mixtures as a function of density from the FMSA and Monte Carlo simulations for $\sigma_2/\sigma_1=0.5$, $\varepsilon_2/\varepsilon_1=0.5$, $T^*=3.0$, $\lambda_{1,1}=\lambda_{1,2}=\lambda_{1,12}=1.8$, $\lambda_{2,1}=4.0$, and $k_1=k_2=1.0$ (case 1). The meaning of the symbols is the same as in Fig. 1.

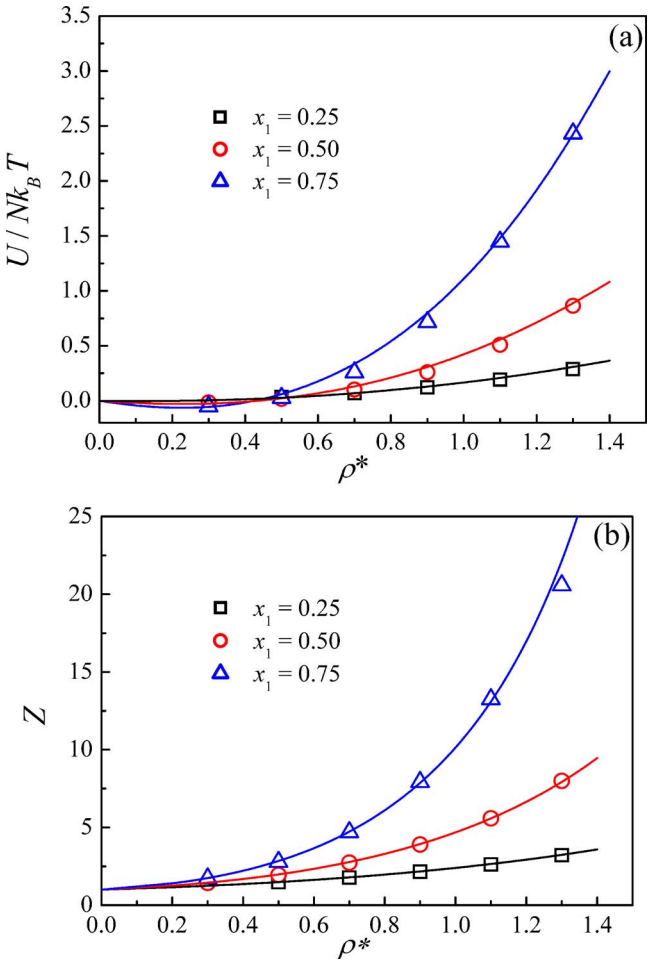

FIG. 6. (Color online) Comparison of (a) internal energy and (b) compressibility factor of binary HCTY mixtures as a function of density from the FMSA and Monte Carlo simulations for $\sigma_2/\sigma_1=0.5$, $\varepsilon_2/\varepsilon_1=0.5$, $T^*=3.0$, $\lambda_{1,1}=\lambda_{1,2}=\lambda_{1,12}=1.8$, $\lambda_{2,1}=8.0$, and $k_1=k_2=-6.0$ (case 2). The meaning of the symbols is the same as in Fig. 1.

$$Z = Z_{hs} + \rho^*(\partial a_1/\partial\rho^*)_{T,N} + \rho^*(\partial a_2/\partial\rho^*)_{T,N}, \tag{24}$$

where $\rho^* = \rho\sigma_1^3$ is the reduced density, and $Z_{\rm hs}$ is the compressibility factor of hard-sphere mixture, which is given by[27]

$$Z_{\rm hs} = \frac{1}{\Delta} + \frac{3\xi_1\xi_2}{\Delta^2\xi_0} + \frac{(3-\xi_3)\xi_2^3}{\Delta^3\xi_0}. \tag{25}$$

The internal energy can be derived from Eqs. (13), (14), and (23). The result is given by

$$U/Nk_BT = a_1 + 2a_2. \tag{26}$$

B. Structural properties

It is known that the MSA predicts good radial distribution functions at large distance, but it behaves worse at short distance. A simplified exponential (SEXP) approximation can be used to improve the accuracy for predicting radial distribution functions. Besides its simplicity and high accuracy, the SEXP approximation for the radial distribution function has strong theoretical basis.[18] Its expression within the FMSA approach is given by

$$g_{ij}(r) = g_{0,ij}(r)e^{g_{1,ij}(r)}, \tag{27}$$

where $g_{0,ij}(r)$ is the radial distribution function of the hard-sphere fluid, and $g_{1,ij}(r)$ is the perturbative one in the FMSA approach. Their expression at contact can be obtained, respectively, from the BMCSL equation of state[27] and the FMSA approach.[10]

$$g_{0,ij}(\sigma_{ij}) = \frac{1}{\Delta} + \frac{\sigma_i\sigma_j}{\sigma_{ij}}\frac{3\xi_2}{2\Delta^2} + \left(\frac{\sigma_i\sigma_j}{\sigma_{ij}}\right)^2\frac{\xi_2^2}{2\Delta^3}, \tag{28}$$

$$g_{1,ij}(\sigma_{ij}) = \frac{\sum_\gamma\sum_l\sum_k K_{\gamma,lk}B_{il}(\lambda_{\gamma,lk})B_{jk}(\lambda_{\gamma,lk})}{2\pi\sigma_{ij}\sqrt{\rho_i\rho_j}}. \tag{29}$$

IV. RESULTS AND DISCUSSION

The *NVT* Monte Carlo simulation results for the radial distribution function at contact $g_{ij}(\sigma_{ij})$, the internal energy U/Nk_BT, and the compressibility factor Z for the binary HCTY mixture are listed in Tables I–VIII at various temperatures $T^*=k_BT/\varepsilon_1$, reduced densities ρ^*, molar fractions x_1, hard-core diameter ratios σ_2/σ_1, and energy parameter ratios $\varepsilon_2/\varepsilon_1$. The comparisons of the theoretically calculated inter-

Author complimentary copy. Redistribution subject to AIP license or copyright, see http://jcp.aip.org/jcp/copyright.jsp

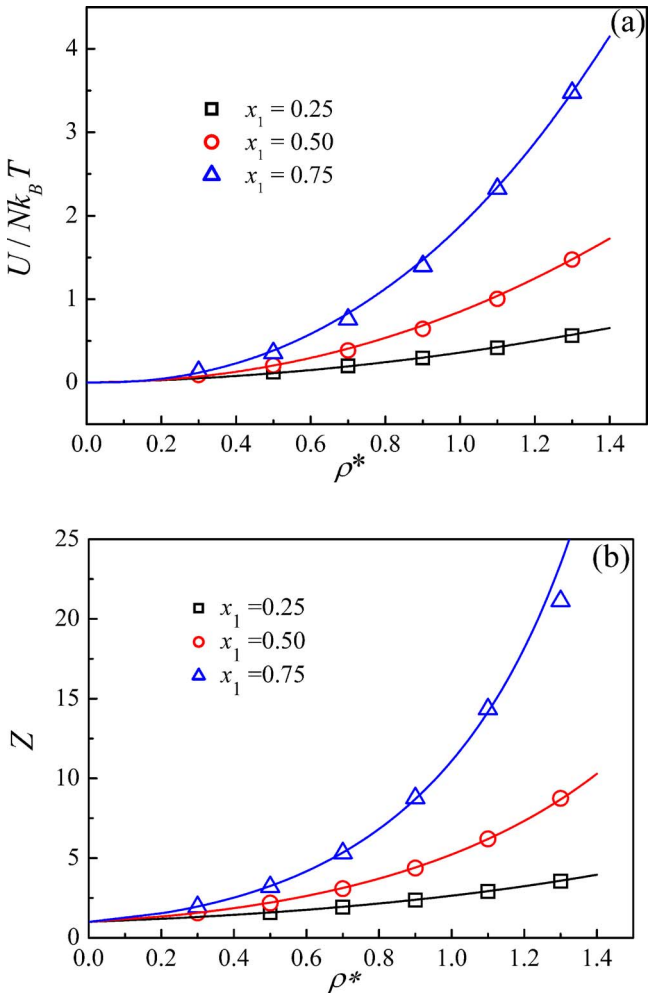

FIG. 7. (Color online) Comparison of (a) internal energy and (b) compressibility factor of binary HCTY mixtures as a function of density from the FMSA and Monte Carlo simulations for $\sigma_2/\sigma_1=0.5$, $\varepsilon_2/\varepsilon_1=0.5$, $T^*=6.0$, $\lambda_{1,1}=\lambda_{1,2}=\lambda_{1,12}=1.8$, $\lambda_{2,1}=8.0$, and $k_1=k_2=-12.0$ (case 3). The meaning of the symbols is the same as in Fig. 1.

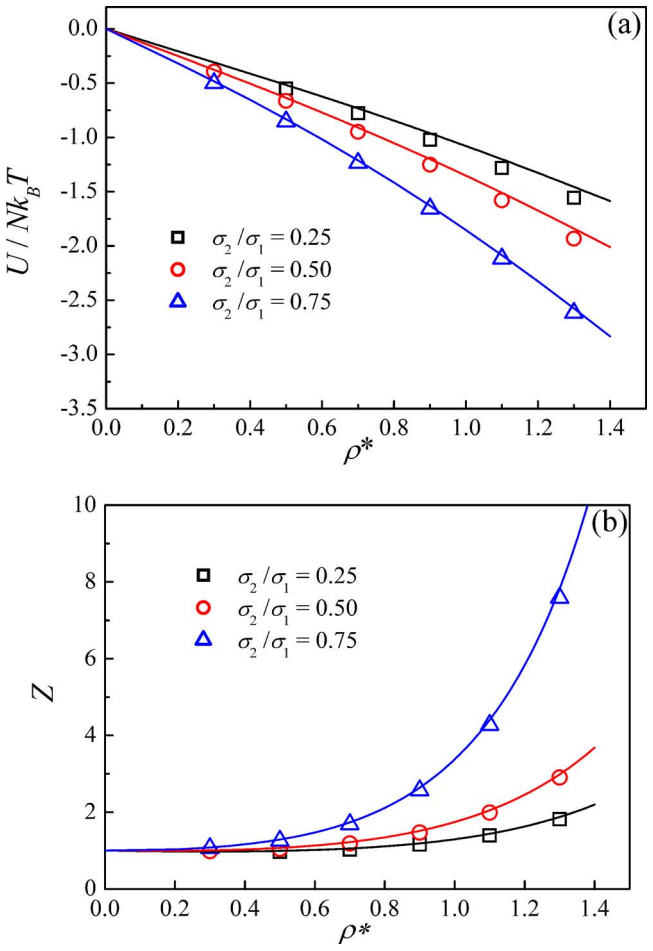

FIG. 8. (Color online) Effect of size ratio on (a) internal energy and (b) compressibility factor of binary HCTY mixtures predicted from the FMSA and Monte Carlo simulations for $\varepsilon_2/\varepsilon_1=0.5$, $x_1=0.5$, $T^*=3.0$, $\lambda_{1,1}=\lambda_{1,2}=\lambda_{1,12}=1.8$, $\lambda_{2,1}=4.0$, and $k_1=k_2=1.0$ (case 1). The meaning of the symbols is the same as in Fig. 1.

nal energy and compressibility factor with the MC simulation data for the binary HCTY mixtures are shown in Figs. 1–8.

Table I presents *NVT* MC results in case 1 for $\sigma_2/\sigma_1=0.5$ and $\varepsilon_2/\varepsilon_1=0.5$. Figure 1 shows a comparison between theory and MC simulation results of internal energy and compressibility factor in case 1 as a function of density at reduced temperatures $T^*=1.5$, 2.0, and 3.0. Theoretical predictions are in very good agreement with MC simulation results at $T^*=2.0$ and 3.0. The predicted internal energy is slightly higher than that of MC simulations at low temperature ($T^*=1.5$). Since in case 1 the interaction outside the hard core is attractive, the internal energy is negative at entire range of temperature and density. The internal energy becomes more negative as reduced temperature is decreased. In the meantime, the compressibility factor decreases as temperature is decreased. This finding is in accordance with that for pure Yukawa fluid in the literature.[16]

Figures 2–4 show comparisons between theory and simulation results of internal energy and compressibility factor for $\sigma_2/\sigma_1=0.5$, $\varepsilon_2/\varepsilon_1=0.5$, and $x_1=0.5$ in cases 2, 3, and 4, respectively. In these cases, the total interaction is repulsive near the contact point but becomes attractive at enough long distance between particles. From Figs. 2 and 3 one can see that in most temperatures and densities, the internal energy is positive, and the compressibility factor increases as temperature is decreased. In case 4, the internal energy and compressibility factor vary similar to case 1 (see Fig. 1) because in both cases, the dominant interaction outside the hard core is attractive force. The theoretical predictions of internal energy and compressibility factor are in good agreement with the MC simulation results except for lower temperatures, where the theory slightly overestimates the internal energy. Also in Figs. 1 and 4, the fluid-fluid equilibria can be found at some low temperatures. However, there is no fluid-fluid equilibrium in cases 2 and 3 due to the fact that the repulsive interaction between particles is dominant at the distance larger than the hard-core diameter σ_{ij}.

Figures 5–7 presents comparisons between theory and MC simulation results of internal energy and compressibility factor of binary HCTY mixtures as a function of molar fraction and density for $\sigma_2/\sigma_1=0.5$ and $\varepsilon_2/\varepsilon_1=0.5$ in cases 1–3, respectively. From Figs. 5–7 one can find that at temperatures studied ($T^*\geqslant 3.0$), the compressibility factor is dominated by the particle size (hard-core diameter), while the

Author complimentary copy. Redistribution subject to AIP license or copyright, see http://jcp.aip.org/jcp/copyright.jsp

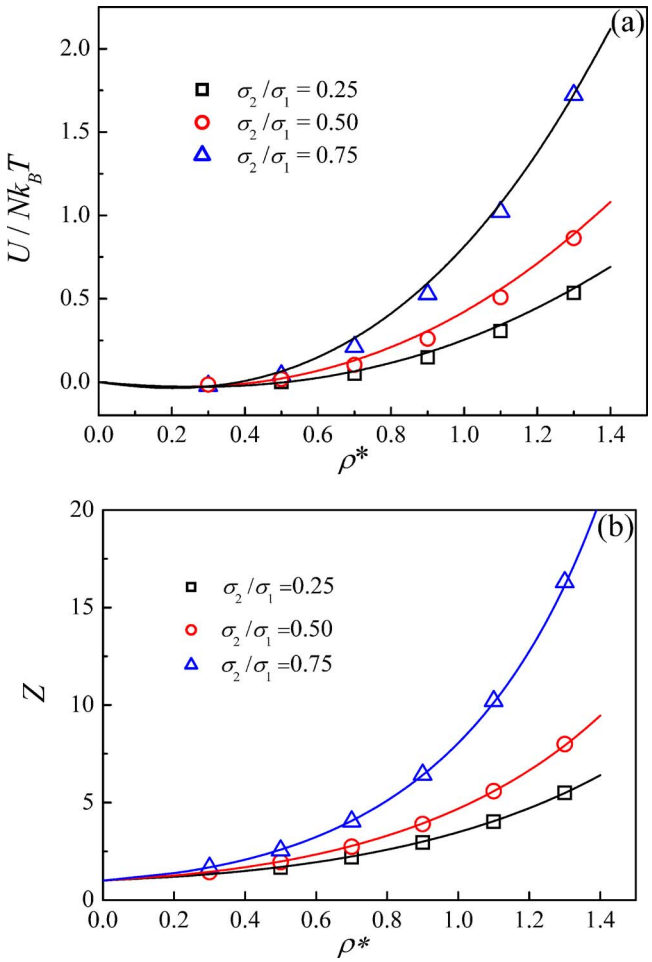

FIG. 9. (Color online) Effect of size ratio on (a) internal energy and (b) compressibility factor of binary HCTY mixtures predicted from the FMSA and Monte Carlo simulations for $\varepsilon_2/\varepsilon_1=0.5$, $x_1=0.5$, $T^*=3.0$, $\lambda_{1,1}=\lambda_{1,2}=\lambda_{1,12}=1.8$, $\lambda_{2,1}=8.0$, and $k_1=k_2=-6.0$ (case 2). The meaning of the symbols is the same as in Fig. 1.

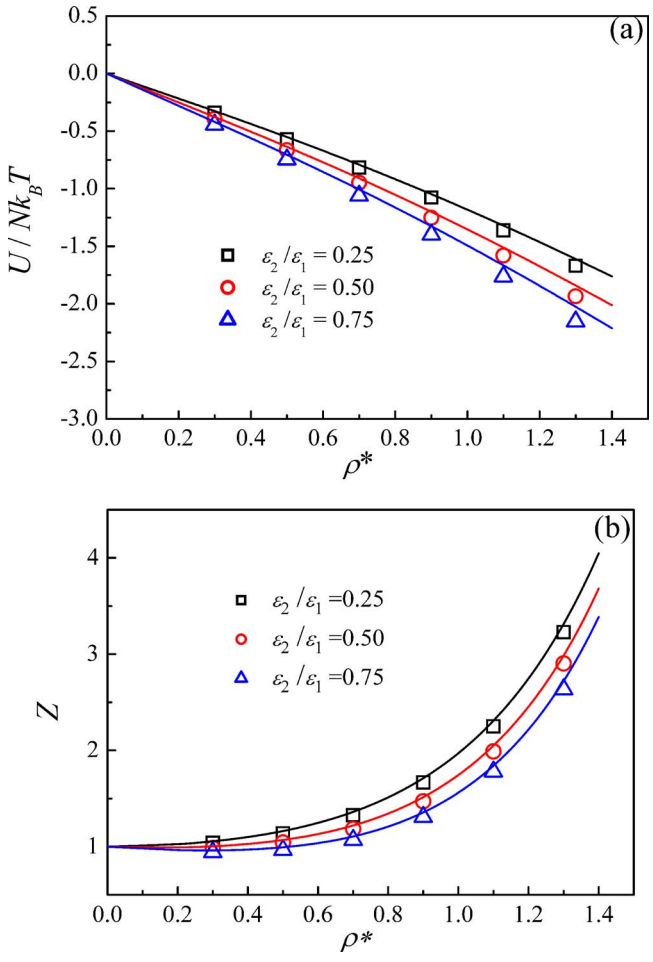

FIG. 10. (Color online) Effect of energy parameter on (a) internal energy and (b) compressibility factor of binary HCTY mixtures predicted from the FMSA and Monte Carlo simulations for $\sigma_{22}/\sigma_{11}=0.5$, $x_1=0.5$, $T^*=3.0$, $\lambda_{1,1}=\lambda_{1,2}=\lambda_{1,12}=1.8$, $\lambda_{2,1}=4.0$, and $k_1=k_2=1.0$ (case 1). The meaning of the symbols is the same as in Fig. 1.

internal energy is dominated by the energy parameter. Because the size of component 1 is larger than component 2, the compressibility factor of the binary HCTY mixture increases as the molar fraction of component 1 is increased. The absolute value of the internal energy also increases as the molar fraction of component 1 is increased due to the energy parameter $\varepsilon_1 > \varepsilon_2$. As can be seen from Figs. 5–7, theoretical predictions are in very good agreement with MC simulation data.

The effects of size ratio on internal energy and compressibility factor of binary HCTY mixtures are listed in Tables IV and V. Figures 8 and 9 show comparisons between theory and MC simulation results of internal energy and compressibility factor of binary HCTY mixtures as a function of size ratio and density for $\varepsilon_2/\varepsilon_1=0.5$, $x_1=0.5$, and $T^*=3.0$ in cases 1 and 2, respectively. It is evident that theoretical predictions are in excellent agreement with MC simulation results for all values of size ratios. Figures 8 and 9 demonstrate that the absolute values of both internal energy and compressibility factor increase with the increase of the particle size.

The effects of energy parameter on internal energy and compressibility factor for binary HCTY mixture in cases 1 and 2 are listed in Tables VI and VII, respectively. From the tables, we found that as the value of energy parameter is increased, the absolute value of internal energy increases. When the total internal energy of the system is positive, the compressibility factor becomes larger with the increase of temperature. A contrary variation tendency of compressibility factor is found when the total internal energy is negative. Figure 10 shows a comparison of the internal energy and compressibility factor predicted from the FMSA approach with that from MC simulations for $\sigma_2/\sigma_1=0.5$, $x_1=0.5$, and $T^*=3.0$ in case 1. This figure shows the energy ratio variation. Again, the analytical theory is in excellent agreement with MC simulation results.

The comparisons of radial distribution functions at contact from the SEXP approximation and MC simulations for binary HCTY mixtures are plotted in Figs. 11 and 12. Figure 11 presents composition variation for $\sigma_2/\sigma_1=0.5$, $\varepsilon_2/\varepsilon_1=0.5$, $T^*=3.0$, $\lambda_{1,1}=\lambda_{1,2}=\lambda_{1,12}=1.8$, $\lambda_{2,1}=4.0$, and $k_1=k_2=1.0$ (case 1), while Fig. 12 shows energy ratio variation for $\sigma_2/\sigma_1=0.5$, $x_1=0.5$, $T^*=3.0$, $\lambda_{1,1}=\lambda_{1,2}=\lambda_{1,12}=1.8$, $\lambda_{2,1}=8.0$, and $k_1=k_2=-6.0$ (case 2). For all the mixtures, the SEXP approach based on the FMSA gives very good results for the radial distribution functions at contact. Figure 13 shows ra-

Author complimentary copy. Redistribution subject to AIP license or copyright, see http://jcp.aip.org/jcp/copyright.jsp

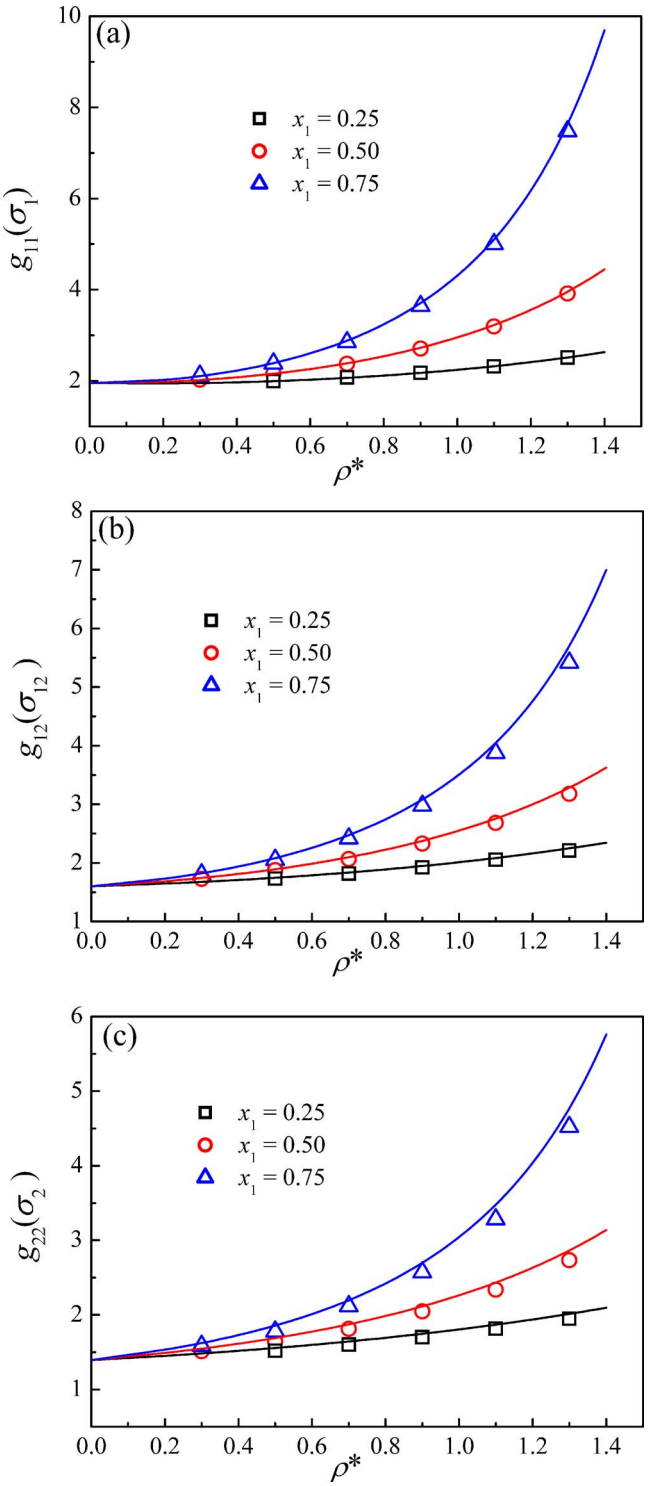

FIG. 11. (Color online) Comparison of radial distribution functions at contact from the SEXP approximation and Monte Carlo simulations for binary HCTY mixture at $T^*=3.0$, $\sigma_2/\sigma_1=0.5$, $\varepsilon_2/\varepsilon_1=0.50$, $\lambda_{1,1}=\lambda_{1,2}=\lambda_{1,12}=1.8$, $\lambda_{2,1}=4.0$, and $k_1=k_2=1.0$ (case 1): (a) $g_{11}(\sigma_1)$, (b) $g_{12}(\sigma_{12})$, and (c) $g_{22}(\sigma_2)$. The symbols and solid lines represent the results from Monte Carlo simulations and SEXP approximation, respectively.

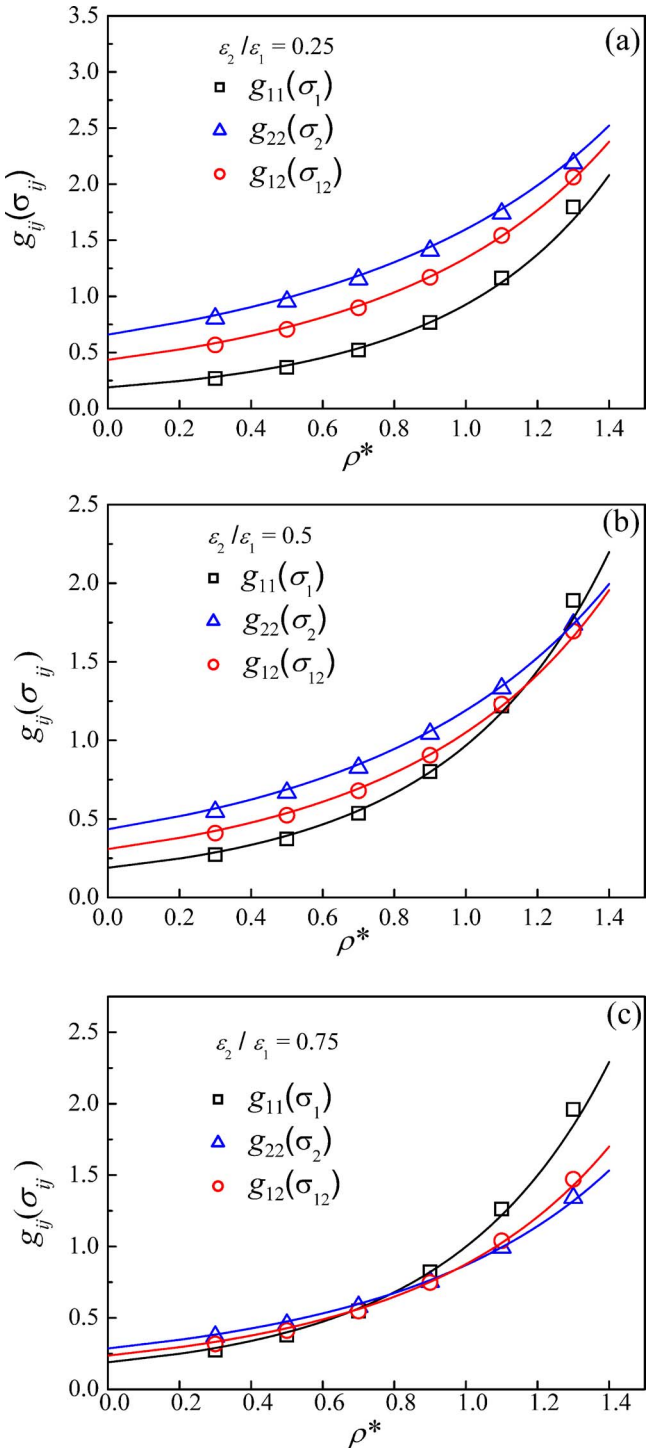

FIG. 12. (Color online) Comparison of radial distribution functions at contact from the SEXP approximation and Monte Carlo simulations for binary HCTY mixture at $T^*=3.0$, $x_1=0.50$, $\sigma_2/\sigma_1=0.5$, $\lambda_{1,1}=\lambda_{1,2}=\lambda_{1,12}=1.8$, $\lambda_{2,1}=8.0$, and $k_1=k_2=-6.0$ (case 2). The meaning of the symbols is the same as in Fig. 11.

dial distribution functions for the binary HCTY mixture as a function of distance at $T^*=6.0$, $\rho^*=1.3$, $\sigma_2/\sigma_1=0.5$, and $\varepsilon_2/\varepsilon_1=0.5$ in case 2. It can be seen from Figs. 11 and 12 that the increase of density results in more frequent contact due to reducing the inert-particle distance. This behavior is the same as pure fluid interacting with a multi-Yukawa potential.

V. CONLUSIONS

Monte Carlo simulation results of internal energy, compressibility factor, and radial distribution function are presented for binary mixed colloids represented by the binary hard-core two-Yukawa mixture under various conditions in the fluid phase. The accuracy of the analytical results from the FMSA for the thermodynamic properties of the binary

Author complimentary copy. Redistribution subject to AIP license or copyright, see http://jcp.aip.org/jcp/copyright.jsp

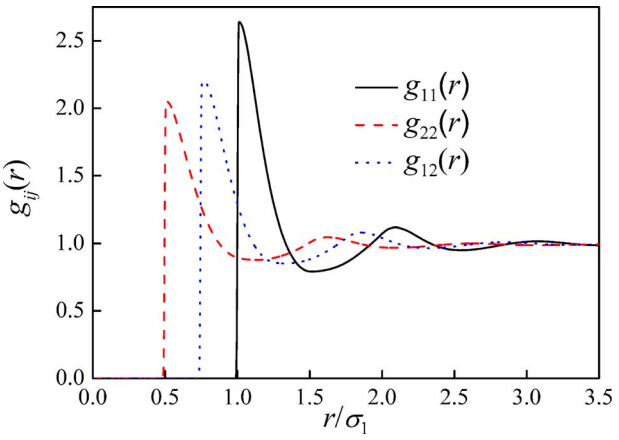

FIG. 13. (Color online) Radial distribution functions of binary HCTY mixtures from the Monte Carlo simulations at $T^*=6.0$, $\rho^*=1.3$, $\sigma_2/\sigma_1=0.5$, $\varepsilon_2/\varepsilon_1=0.5$, $\lambda_{1,1}=\lambda_{1,2}=\lambda_{1,12}=1.8$, $\lambda_{2,1}=8.0$, and $k_1=k_2=-6.0$ (case 2).

HCTY model fluid has been assessed against MC simulation data. The general agreement of the predictions from the FMSA with the simulation results is quite satisfactory. The effects of temperature, density, composition, size and energy ratios on internal energy, and compressibility factor have been investigated extensively for the binary HCTY model fluid. The FMSA predicts these effects very well and is capable of describing the fluid-fluid phase transition of the binary HCTY fluids at low temperature. Furthermore, we found that for the binary HCTY mixtures, the SEXP approximation based on the FMSA is quite accurate in prediction of the radial distribution functions at contact.

It is believed that the binary HCTY fluid model possesses a wide range of application due to its ease of use and its ability to capture crucial features of real fluids.[21] The FMSA described here is most promising for describing the thermodynamic and structural properties of mixed colloids, mixed globular proteins in electrolyte solution, dusty plasmas, etc.

ACKNOWLEDGMENTS

This work is supported by the National Natural Science Foundation of China under Grant No. 20676065 and the program for New Century Excellent Talents in University (NCET) of China.

[1] A. R. Leach, *Molecular Modeling: Principles and Applications*, 1st ed. (Addison-Wesley Longman, 1996).
[2] K. P. Shukla, J. Chem. Phys. **112**, 10358 (2000).
[3] R. T. Farouki and S. Hamahuichi, J. Chem. Phys. **101**, 9885 (1994).
[4] M. Bonaskarne, S. Amokrane, and C. Regnaut, J. Chem. Phys. **111**, 2151 (1999).
[5] L. Jin, Y.-X. Yu, and G.-H. Gao, J. Colloid Interface Sci. **304**, 77 (2006).
[6] Y. Liu, E. Fratini, P. Baglioni, W. R. Chen, and S.-H. Chen, Phys. Rev. Lett. **95**, 118102 (2005).
[7] M. Hasegawa, J. Chem. Phys. **108**, 208 (1998).
[8] Y.-X. Yu, A.-W. Tian, and G.-H. Gao, Phys. Chem. Chem. Phys. **7**, 2423 (2005).
[9] Y. Liu, W.-R. Chen, and S.-H. Chen, J. Chem. Phys. **122**, 044507 (2005).
[10] Y. P. Tang, Mol. Phys. **100**, 1033 (2002).
[11] E. Waisman, Mol. Phys. **25**, 45 (1973).
[12] L. Blum and J. S. Høye, J. Stat. Phys. **19**, 317 (1978).
[13] D. Henderson, L. Blum, and J. P. Noworyta, J. Chem. Phys. **102**, 4973 (1995).
[14] J. H. Herrera, H. Ruiz-Estrada, and L. Blum, J. Chem. Phys. **104**, 6327 (1996).
[15] L. Mier-y-Teran, S. E. Quinones-Cisneros, and I. D. Nunez-Riboni, J. Chem. Phys. **95**, 179 (1998).
[16] Y.-Z. Lin, Y.-G. Li, J.-F. Lu, and W. Wu, J. Chem. Phys. **117**, 10165 (2002).
[17] P. Prinsen, J. C. Pamies, T. Odijk, and D. Frenkel, J. Chem. Phys. **125**, 194506 (2006); A. Fortini, A.-P. Hynninen, and M. Dijkstra, J. Chem. Phys. **125**, 094502 (2006); Y. Duda, A. Romero-Martinez, and P. Orea, J. Chem. Phys. **126**, 224510 (2007).
[18] T. W. Cochran and Y. C. Chiew, J. Chem. Phys. **121**, 1480 (2004).
[19] H. Guerin, Physica A **304**, 327 (2002).
[20] Y. P. Tang, Y.-Z. Lin, and Y.-G. Li, J. Chem. Phys. **122**, 184505 (2005).
[21] M. Broccio, D. Costa, Y. Liu, and S.-H. Chen, J. Chem. Phys. **124**, 084501 (2006).
[22] E. Arrieta, C. Jedrzejek, and K. N. Marsh, J. Chem. Phys. **95**, 6806 (1991).
[23] E. Scholl-Paschinger, D. Levesque, J.-J. Weis, and G. Kahl, J. Chem. Phys. **122**, 024507 (2005).
[24] A. Giacometti, D. Gazzillo, G. Pastore, and T. K. Das, Phys. Rev. E **71**, 031108 (2005).
[25] V. J. Anderson and H. N. W. Lekkerkerker, Nature (London) **416**, 811 (2002); J. C. Gabel, R. L. Scott, T. H. Admir, R. E. Drake, and D. L. Traber, Am. J. Physiol. Heart Circ. Physiol. **239**, H810 (1980).
[26] D. A. McQuarrie, *Statistical Mechanics* (Harper & Row, New York, 1976).
[27] T. Boublik, J. Chem. Phys. **53**, 471 (1970); G. A. Mansoori, N. F. Carnahan, K. E. Starling, and T. W. Leland, J. Chem. Phys. **54**, 1523 (1971).

Author complimentary copy. Redistribution subject to AIP license or copyright, see http://jcp.aip.org/jcp/copyright.jsp